Hindawi Publishing Corporation
Advances in Materials Science and Engineering
Volume 2016, Article ID 2156936, 13 pages
http://dx.doi.org/10.1155/2016/2156936

Research Article

The Deformation Mechanisms in Process of Crack Propagation for Alpha Titanium with Compounding Microdefects

Ying Sheng and Xiang-guo Zeng

College of Architecture and Environment, Sichuan University, Chengdu 610065, China

Correspondence should be addressed to Xiang-guo Zeng; xiangguozeng@scu.edu.cn

Received 26 February 2016; Revised 22 May 2016; Accepted 23 May 2016

Academic Editor: Hiroshi Noguchi

The multiscale analysis method based on traction-separation law (TSL) and cohesive zone law was used to describe the cross-scale defective process of alpha titanium (α-Ti) material with compounding microdefects in this paper. First, the properties of T-S curve and the reasonable range of T-S area relative to the length of defects were discussed. Next, based on the conclusions above, the molecule dynamics analysis of three models of α-Ti with compounding microdefects was conducted and cross-scaly simulated. The phenomenon, principles, and mechanisms of different compound microscale defects propagation of α-Ti were observed and explained at atomic scale, and the effects of different microdefects on macrofracture parameters of materials were studied.

1. Introduction

Microdefects commonly occur on materials. Microdefects of materials not only occur during the manufacture and fabrication process, but also form new microdefects under different loading circumstances. For example, micro tip cracks will occur under fatigue loading, and voids or micro blunt cracks will occur under impact loading [1]. And the material properties strongly depend on the atom structure and microstructure of itself [2]. Hence, in order to improve the security of materials during practical application, it is significant to study the effect of microdefects on macrocharacteristics of materials.

How to build proper models and find methods to carry out cross-scale analysis on the micro and macroproperties of materials becomes central attention of many scholars. Currently, there are two classic research methods: the serial multiscale method and the parallel multiscale method. For the serial method, the numerical model of mesoscale elements needs to be built first, then based on the micro numerical results, the macrostructure parameters can be estimated according to the multiscale theories, and finally the obtained parameters can be applied to macrostructure simulation by some methods, such as homogenization method [3]. For the parallel method, the micro and macro numerical models can be built simultaneously, and then different cross-scale methods can be used to connect and exchange data between macro and micro models, such as Macroscopic/Atomistic/Ab initio Dynamics (MAAD) method [4], Quasi Continuum (QC) method [5], and coarse-grained molecular dynamics (CGMD) method [6].

There are mainly two types of models to study crack propagation and fracture problems: one is based on classical fracture mechanics models and the other is based on damage mechanics models. Among them, the cohesive method based on damage mechanics is one of the widely applied methods. It applies to both macrocrack propagation and microcrack propagation [7, 8]. The basic ideas of the cohesive method are applying traction-separation law (TSL) to simulate cohesive forces among atomic lattice and therefore avoid singularity of crack tip and adopting cohesive separation principles to define the properties of cohesive interface elements. The cohesive separation principles include cohesive plastic property, cohesive elastic property, fracture, fiber damage, mechanics defect, circular loading defect, and other behaviors. The cohesive method is appropriate to apply to concrete, metals, compound materials, and many other materials. Houachine et al. [9] applied the cohesive method to successfully predict the interface integrate stress of FRP and concrete beam; Kebriaei et al. [10] used the cohesive method to build

multiscale model of AA1050 and AA5754 alloy connection and described integrate properties of connection interface. Grogan et al. [11] used the cohesive method to successfully simulate the formation and propagation of microcracks of composite laminates materials.

However, what is the optimum range of T-S region related to the length of the initial crack is also an open issue. If T-S area exceeds the affected range of the crack too much, it will not only increase meaningless computation because of the unreasonable model, but also make the traction value obtained through computation less than real value. If the value of T-S area is too small, then it is unable to accurately evaluate the impact of microcrack propagation on macromechanics performance of the material. In order to carry out quantitative evaluation on crack's impact area at microscale and provide evidence to confirm the reasonable T-S area, this paper discussed the properties of T-S curve as well as reasonable range of T-S area relative to the defect length first by taking α-Ti material as an example.

Ti alloy has several advantages such as high stress, small density, corrosion resistance, and good deform property under low temperature. That is why it is widely used in aviation, shipping, mechanic production, and weapon industry and also frequently endures high-speed impact loading during its application [12]. Ti has allotropism phenomenon. Under the temperature of 882°C, it becomes hexagonal crystal packed (HCP) structure, and it is also called α-Ti. α-Ti is an anisotropic material and its mechanical properties of different crystal orientation are different. In this paper, taking α-Ti material as an example, the traction-separation law (TSL) method was adopted to discuss the properties of T-S curve as well as the reasonable range of T-S area relative to the defect length. Then based on the conclusions, the open source code of LAMMPS [13] developed by Sandia laboratory was adopted to analyze the molecule dynamics of the three models of α-Ti with compound microdefects, and AtomEye software [14] was also used to carry out the visualization of the atom configuration during the process of deformation. In addition, the different compound microdefects propagation phenomenon, principles, and mechanisms of α-Ti were also observed and explained at atomic scale. Finally, the cohesive zone law multiscale analysis method was adopted to study the effects of different microdefects on macrofracture parameters of materials.

2. Multiscale Simulation Methods

2.1. Brief Review of Molecular Dynamics. Molecular Dynamics (MD) method is one of simulation methods widely used for molecular systems. In the MD method the initial distribution is random, and every new distribution is derived from the previous one by using the interactions between the particles. Consider one particle i in the system. Every other particle j attracts or repels it. The interaction depends on the positions of the particles $\vec{r}_i$ and $\vec{r}_j$ and contributes to the total potential energy of particle:

$$u(\vec{r}_i) = \sum_j u_{ij}(\vec{r}_i, \vec{r}_j). \tag{1}$$

In that potential the particle feels a force

$$\vec{f}_i = -\nabla u(\vec{r}_i) \tag{2}$$

which accelerates the particle in a certain direction.

The forces are used to calculate the velocity of each particle and the new distribution is obtained through Newton's second law:

$$m\vec{a}_i = m\frac{\partial \vec{v}_i}{\partial t} = m\frac{\partial^2 \vec{r}_i}{\partial t^2} = \vec{f}_i, \tag{3}$$

where $\vec{v}_i$ is the velocity of the particle. When the velocity $\vec{v}_i$ of each particle at a given time is calculated by solving the equation of motion (3), one allows every particle to move with that velocity a short period of time and then reevaluates the potential energy, force, and thus the velocity.

The MD method follows classical mechanics of motions and is therefore purely deterministic. It has a real time coordinate and the trajectory therefore follows the changes of the system in time. It is not limited to systems at equilibrium but can be used to study systems under external perturbations.

2.2. Traction-Separation Laws in Cohesive Zone Models. The idea for the cohesive model is based on the consideration that infinite stresses at the crack tip are not realistic. Models to overcome this drawback have been introduced by Dugdale [15] and by Barenblatt [16] for the first time. The material separation and thus damage of the structure are classically described by interface elements, and no continuum elements are damaged in the cohesive model. The behavior of the material is spitted in two parts, the damage-free continuum with an arbitrary material law and the cohesive interfaces between the continuum elements, which specify only the damage of the material. The interface elements open when damage occurs and lose their stiffness at failure so that the continuum elements are disconnected. For this reason the crack can propagate only along the element boundaries.

The separation of the cohesive interfaces is calculated from the displacement jump $[u]$, that is, the difference of the displacements of the adjacent continuum elements,

$$\delta = [u] = u^+ - u^-. \tag{4}$$

The separation depends on the normal and the shear stress, respectively, acting on the surface of the interface. When the normal or tangential component of the separation reaches a critical value, δ_0^N or δ_0^T, respectively, the continuum elements initially connected by this cohesive element are disconnected, which means that the material at this point has failed.

Beside the critical separation δ_0, the maximum traction (stress at the surface of the continuum element) T_0 is used as a fracture parameter, also denoted as cohesive stress. The value of T_0 only describes the maximum value of a traction-separation curve $T(\delta)$, in the following denoted as cohesive law. Like the separations, the stresses T can also act in normal or in tangential direction, leading to normal or shear fracture, respectively. The shape of the curve $T(\delta)$, which is assumed to be a material independent cohesive law, is defined differently by various authors [15, 17, 18].

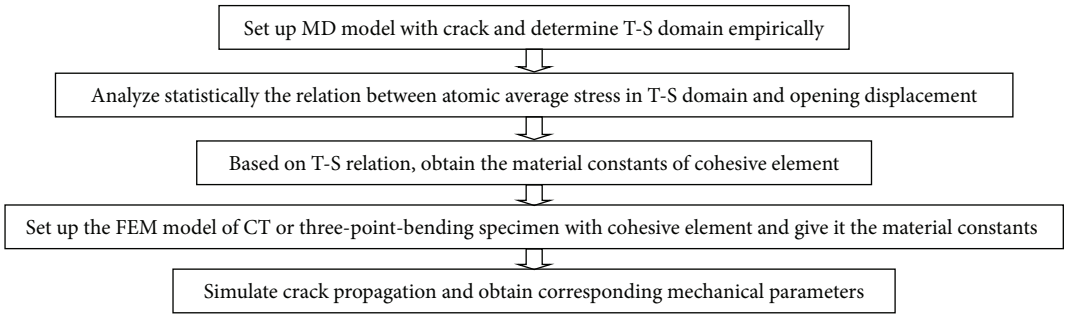

Figure 1: Multiscale analysis flowchart based on cohesive element.

The integration of the traction over separation, either in normal or in tangential direction, gives the energy dissipated by the cohesive elements, Γ_0:

$$\Gamma_0 = \int_0^{\delta_0} T(\delta)\, d\delta. \quad (5)$$

Beside the form of the T-S curve, which was assumed to be a model quantity, there are two material parameters, that is, the maximum separation stress T_0, which has to be overcome for final fracture, and the separation at failure δ_0. These quantities define the height and the width of the curve and give (together with the function of the curve) the dissipated energy per cohesive element as a result.

2.3. Multiscale Simulation Process. Taking the material of α-Ti as an example, our approach studying crack propagation includes the use of MD simulation to obtain T-S relations in cohesive elements. In our present work, the crack propagation of compact tension (CT) model containing cohesive elements, whose T-S relation was derived from MD simulations, is simulated. The method may be called the atomic based cohesive zone models (CZM) method. These results enable us to make several recommendations to improve the methodology to obtain cohesive laws and better comprehend the crack propagation behavior of α-Ti.

The multiscale analysis flow based on cohesive elements is displayed in Figure 1.

3. Results and Discussion

3.1. Evaluation of T-S Region. The cohesive laws, or so-called traction-separation laws (TSL), were introduced into finite element computations for brittle material failure analysis more than 30 years ago [19] and have been used for simulating crack initiation and propagation along interfaces [20] generally in ductile materials for the past decades. However, what is the optimum range of T-S region related to the length of the initial crack is also an open issue.

In order to carry out quantitative evaluation on crack's impact area at microscale and provide evidence to confirm the reasonable T-S area, two micromechanics models with defects of α-Ti material were built: one was with blunt crack defect and the other was with sharp crack defects. The elemental crystal structure of α-Ti is closed-packed hexagonal, as illustrated in Figure 2. The cell parameters of α-Ti are $a = b = 2.95$ Å, $c/a = 1.587$. The slip plane and slip direction of α-Ti are, respectively, {0001} and ⟨1120⟩. There are 12 slip systems in α-Ti, including 3 basal slip systems, 3 prismatic slip systems, and 6 pyramidal slip systems. In both of the crack models, the crack plane is parallel to the crystal plane $(10\bar{1}0)$.

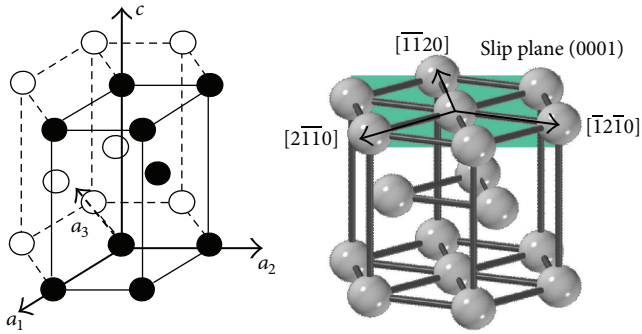

Figure 2: The elemental crystal structure and slip plane of α-Ti.

In order to make the comparison of computational results of the two models, the models were set with similar geometrical parameters and mechanics conditions. The length, width, and thickness of the two models were separately 250 Å, 100 Å, and 3 Å, and the lengths of the sharp crack and the blunt crack were both 25 Å (the width of the blunt crack was 25 Å). The tensile displacement load on both upper and lower surfaces of the two models was 0.25 Å/ps. The range of 10 Å from upper and lower surfaces of the crack was taken as the range of T-S area. The T-S data area was divide into 20 judgement areas along the length direction of T-S data area, which means the maximum judgement precision of effective T-S area was 0.5 times crack length, as shown in Figure 3.

After loading was done, the T-S curves of the two models in all the judgement areas defined in Figure 3 were got, and the similarities and differences of all the T-S curves could be obtained, as shown below.

(1) The T-S curves of the 1st and 2nd areas (bottom of crack) are very similar. In both of the two areas, T-S curves show random status, and the atomic stress is relatively low.

(2) The T-S curves from the 3rd to the 12th areas are similar. All the T-S curves in these areas consist of rise period

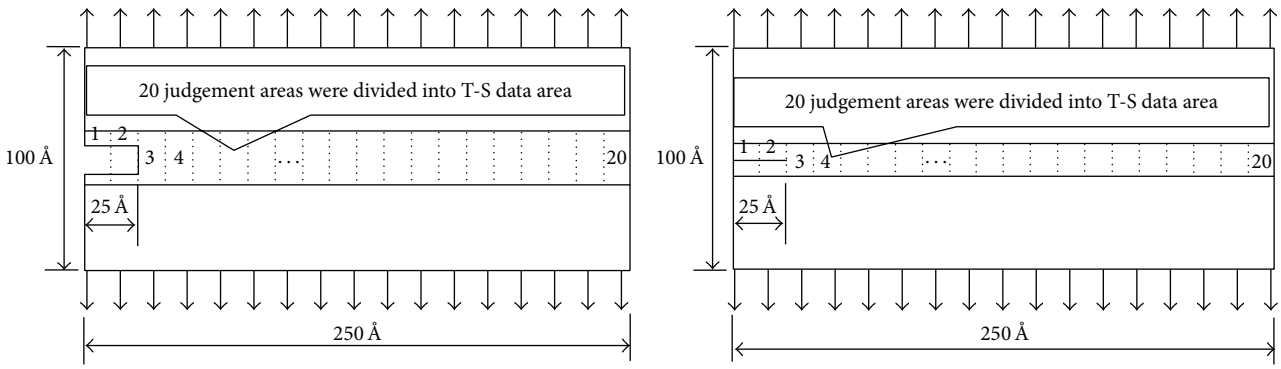

(a) Model with blunt crack defect

(b) Model with sharp crack defect

Figure 3: Two defected micromechanics models.

and drop period, although the maximum atomic stresses of these T-S curves are not exactly the same.

(3) The T-S curves from the 13th to the 20th areas are similar. In these areas, T-S curves only show rising period.

Therefore, the T-S curves of the two models in the representative areas such as the 1st, the 3rd, the 12th, the 13th, the 20th, and the 1st~12th were shown in Figures 4 and 5.

Figures 4 and 5 can lead to the following conclusions.

(1) Within effective impact area of the crack, a T-S curve consists of rise period and drop period. According to the atomic configuration diagrams in Figures 4(f) and 5(f), the complex deformation mechanisms of the crack tip (such as dislocation and blunting) are comprehensively reflected in the T-S curves. Before the T-S curves reach the first peak, the crystal lattice size is changing, but nearly no metallic bond breaks. However, in stress drop period, the blunting of the crack tip and material damage are obvious.

(2) Within the effective impact area of the crack, the maximal stress is related to crack forms and distance between the area and the crack, which means when metallic bonds start to break, the critical stress is not only related to micro-properties of the atoms and atomic bonds, but also related to the crack form and distance between the area and the crack.

(3) Along the direction of crack propagation and within the effective impact area of the crack, when the distance between the area and the crack tip increases, the gradient of T-S curve in the stress drop period is increasing first but decreasing later, which means the speed of metallic bond break is fast first and slow later. The biggest gradient area in the stress drop period of T-S curve is not in the area of the crack tip, but in the area in front of the crack tip.

(4) Within the less affected area by the crack, T-S curve only shows rising period, which means within this part of area, deform is in the elastic period and should not be included in the scope of T-S curve.

(5) Within the less affected area by the crack, the further away from the crack, the smaller the maximal stress, which means the less being affected by the crack. If this part of area is included into the scope of T-S curve, the traction value obtained through computation will be less than the real value, which is unreasonable.

(6) Regardless of the blunt crack or the sharp crack, the impact area of the crack is approximately 6 times the length of the crack, which means the reasonable T-S area should be within the range of 6 times the length of the crack.

3.2. Molecule Dynamics Computational Results of Three Mechanics Models with Compound Defects. Through microscopic observation of tensile and fatigue fracture process, void, blunt crack, and sharp crack can be found in the microstructure of α-Ti [21], as shown in Figure 6.

Before using cohesive elements to simulate crack propagation, the relationship between the interface cohesive force and the crack opening displacement should be obtained first. Three mechanics models with compound defects of α-Ti were used to conduct molecule dynamics computation. Model I was about a boundary blunt crack (main defect) with a void (secondary defect) at its front end; Model II is about a boundary blunt crack (main defect) with a sharp crack (secondary defect) at its front end; Model III is about a boundary sharp crack (main defect) with another sharp crack (secondary defect) at its front end.

In order to make comparison among the three models, similar geometrical parameters and mechanics conditions were assigned to the three models. The sizes of the models were 330 Å × 100 Å × 3 Å; the length of the main defect was 25 Å (the width of the main defect of Model I and Model II was 5.2 Å); the distance between the main defect and the secondary defect was 20.15 Å; the diameter of the secondary defect of Model I was 6 Å, and the length of the secondary defect of Model III was 10 Å. Next, the tensile displacement load on both upper and lower surfaces of the three models was all 0.25 Å/ps. The range of 10 Å from upper and lower surfaces of the crack was taken as the range of T-S area. Then the three molecule dynamics models with compound defects could be built as shown in Figure 7.

Figures 8, 9, and 10 were T-S curves of Model I, Model II, and Model III, respectively, which were obtained through molecule dynamics simulation. At any time, the crack opening displacement corresponded to a discrete point in the T-S curve and an atomic configuration diagram, so the complex deformation mechanisms of the crack tip could be comprehensively reflected in the T-S curves. In order to

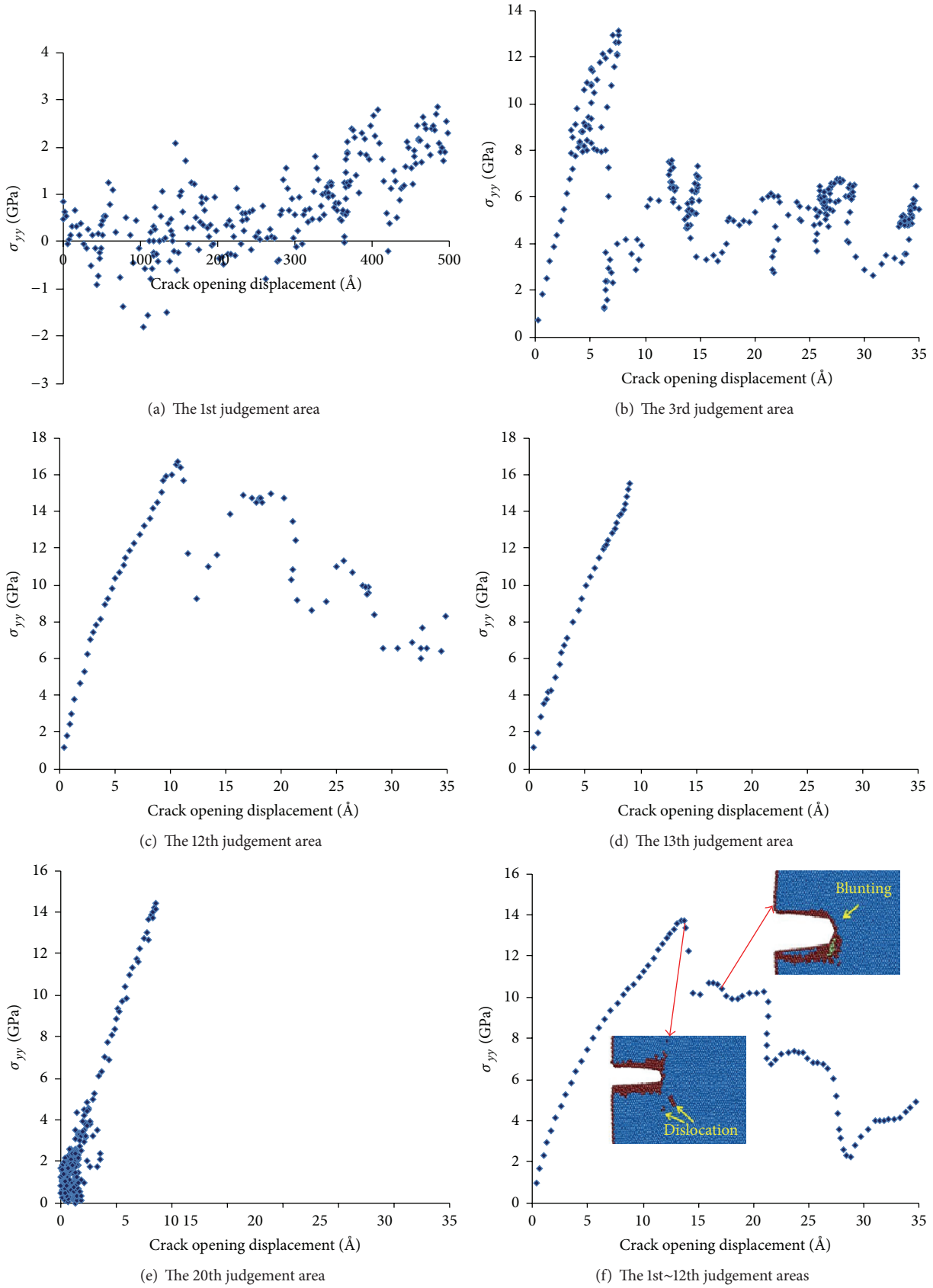

(a) The 1st judgement area

(b) The 3rd judgement area

(c) The 12th judgement area

(d) The 13th judgement area

(e) The 20th judgement area

(f) The 1st~12th judgement areas

Figure 4: T-S curve of the model with blunt crack defect.

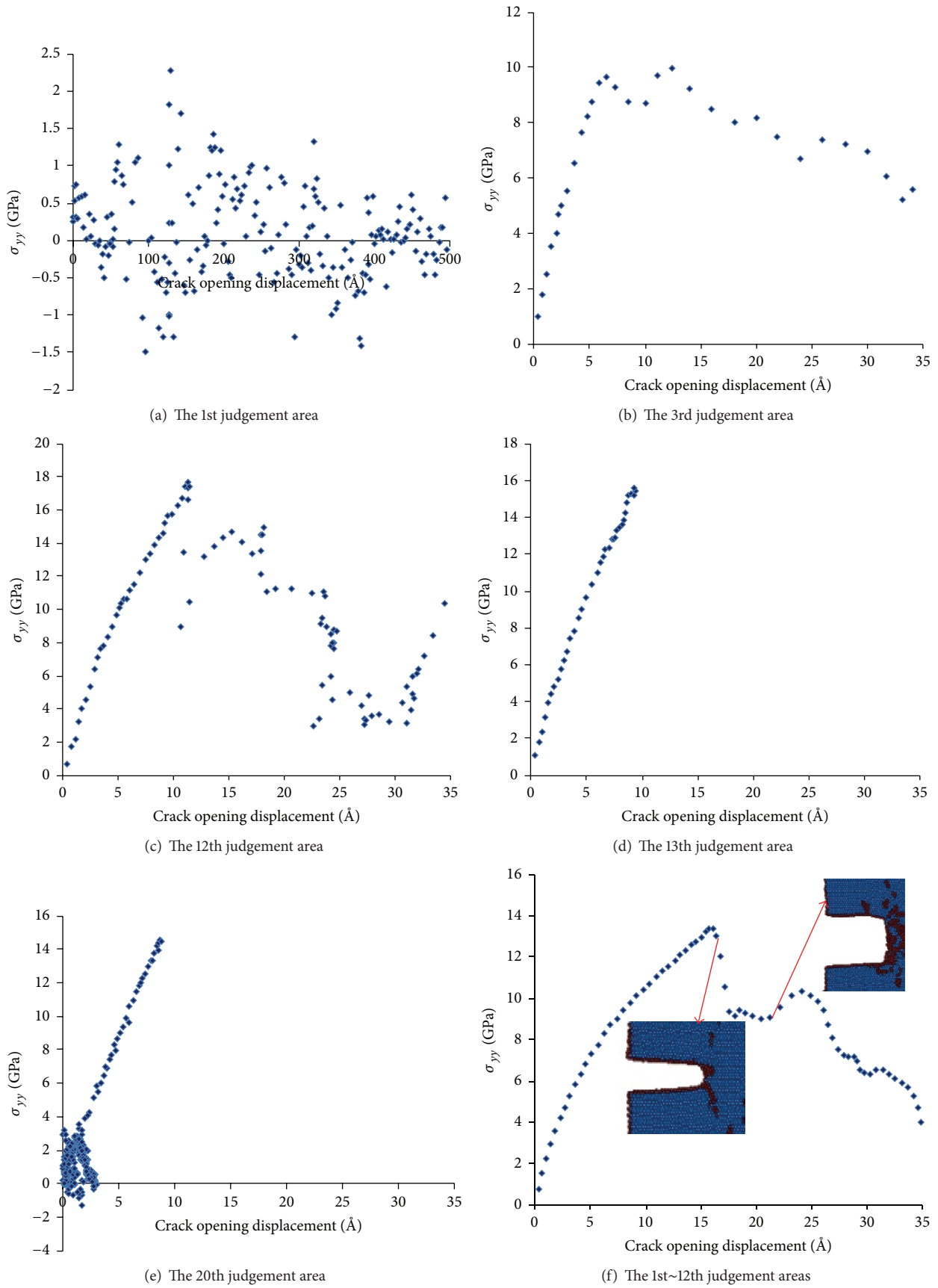

Figure 5: T-S curve of the model with sharp crack defect.

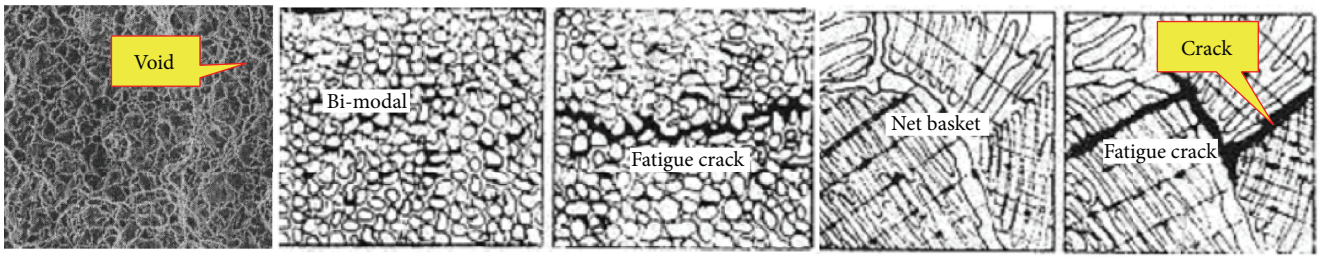

Figure 6: Microstructure of tensile and fatigue fracture surfaces of α-Ti.

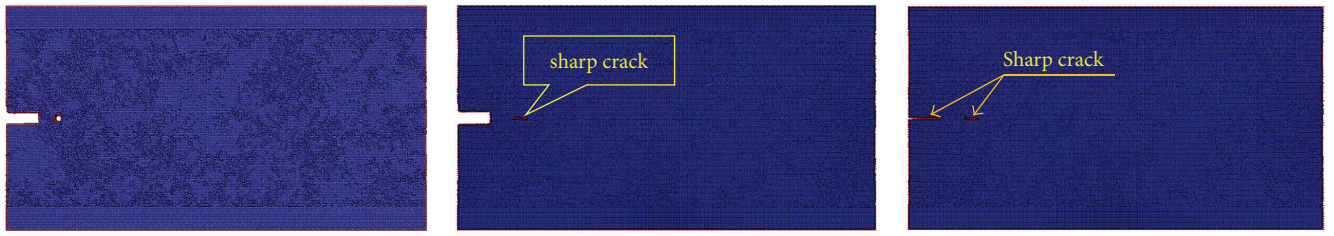

(a) Model I (b) Model II (c) Model III

Figure 7: Three molecule dynamics model with compound defects.

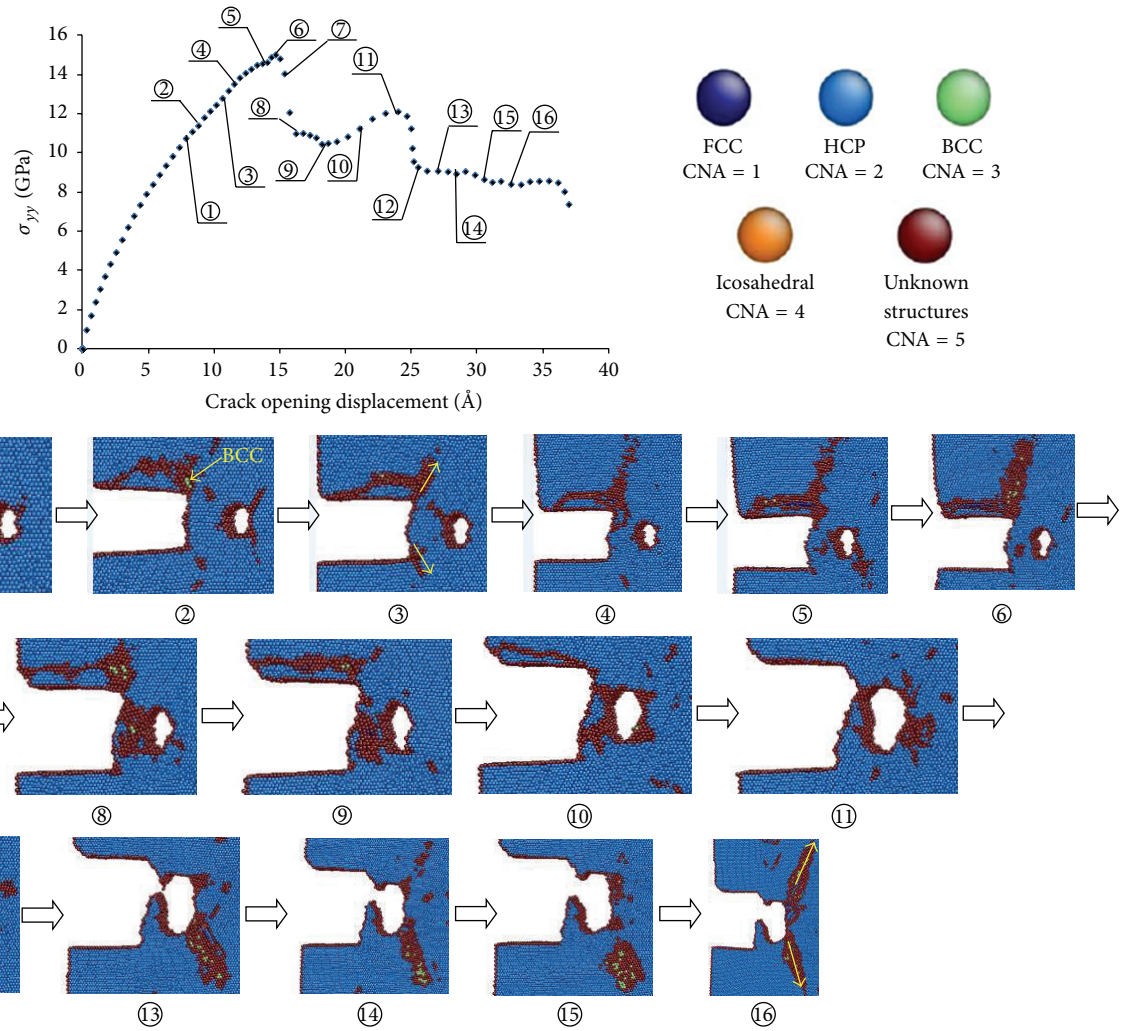

Figure 8: Traction-separation relationship and deformed mechanisms of Model I under tensile loading.

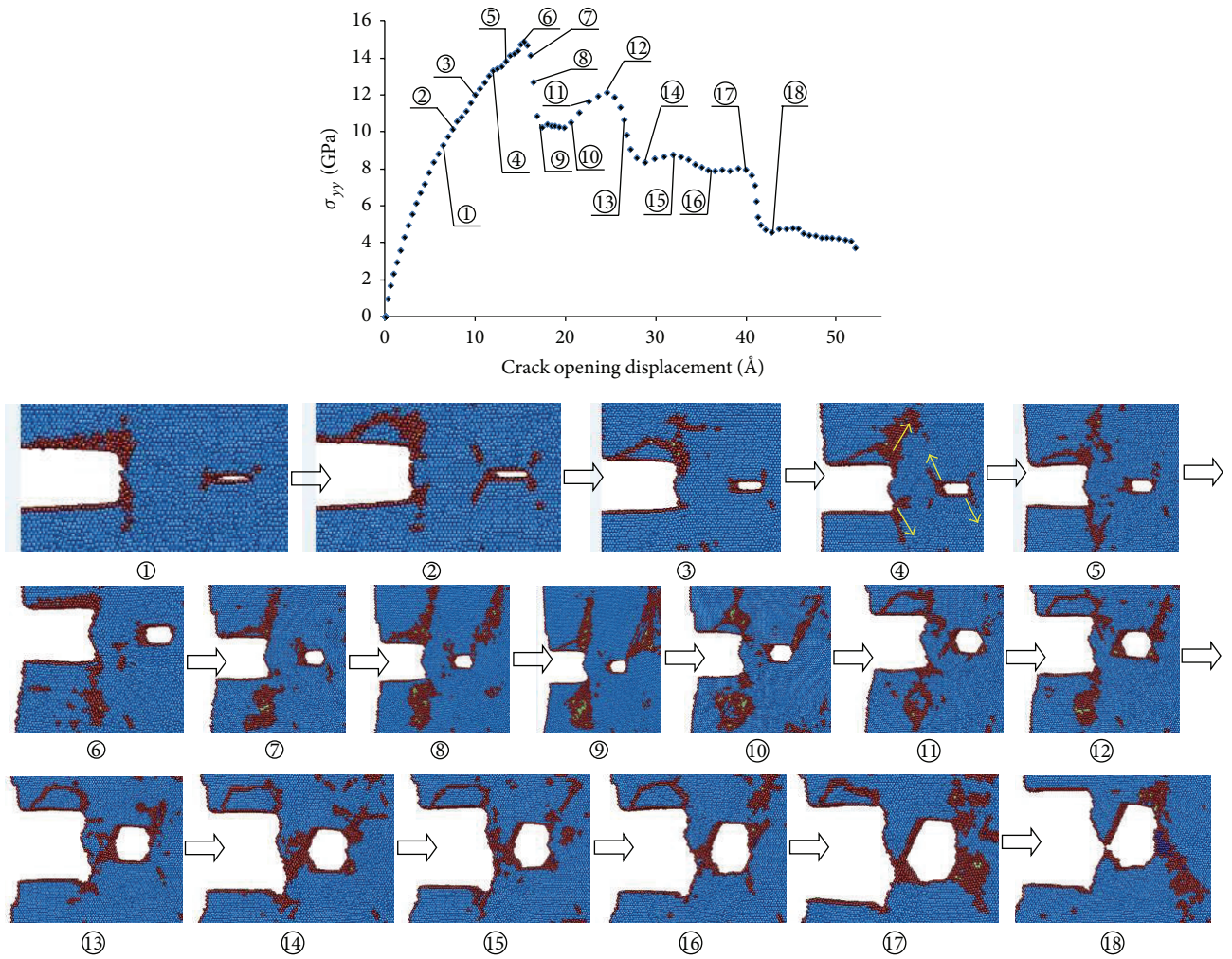

Figure 9: Traction-separation relationship and deformed mechanisms of Model II under tensile loading.

observe the impact of microchange (such as dislocation, crack blunting, phase transition, connection of the main defects, and the secondary defects) on T-S curve, the atom structure drawings corresponding to the key turning points in the curve were highlighted. The atom structure drawings were got by AtomEye software, and different colors of atoms mean different CNA values representing different phases. The color responding to the phase was explained in Figure 8.

Figures 8, 9, and 10 can lead to the following conclusions.

(1) The crack tip's deformation process of Model I is shown in Figure 8. Its crack tip deformation and failure mechanism are bluntness and dislocation emission (as shown in Figures 8③ and 8⑮, the arrow pointing to the direction of dislocation emission). In Model I, when T-S curve approaches the peak value, the stress of the crack tip shows high concentration, the dislocation area expands obviously, and phase transition (BCC) occurs. With further expanding of bluntness, parts of the connecting atoms near the main and secondary defects start to show random status, and the stress declines rapidly. Before full connection of the main and secondary defects, stress should have a temporary small amount of increase. When all the connecting atoms of the main and secondary defects show random status (such as in Figure 8⑪, the red atoms between the main and secondary defects, CAN = 5), stress should reach the second top value. With further loading, stress relaxes and crack propagation slows down, until full connection of cracks.

(2) The crack tip deformation process of Model II is shown in Figure 9. The crack tip deformation and failure mechanism are bluntness and dislocation emission, such as in Figure 9④, and dislocation emission occurs in both the main and secondary defects (arrow pointing to the direction of dislocation emission). In Model II, when T-S curve approaches its peak value, the stress concentration on the crack tip occurs. As the bluntness gets more serious, dislocation area keeps expanding, along with the occurrence of phase transition (BCC), and stress declines rapidly. With continue loading, part of the connecting atoms of the main and secondary defects show random status, and stress slightly increases but is followed by another rapid decline; when large amount of connecting atoms of the main and secondary defects show random status, as further loading, stress should

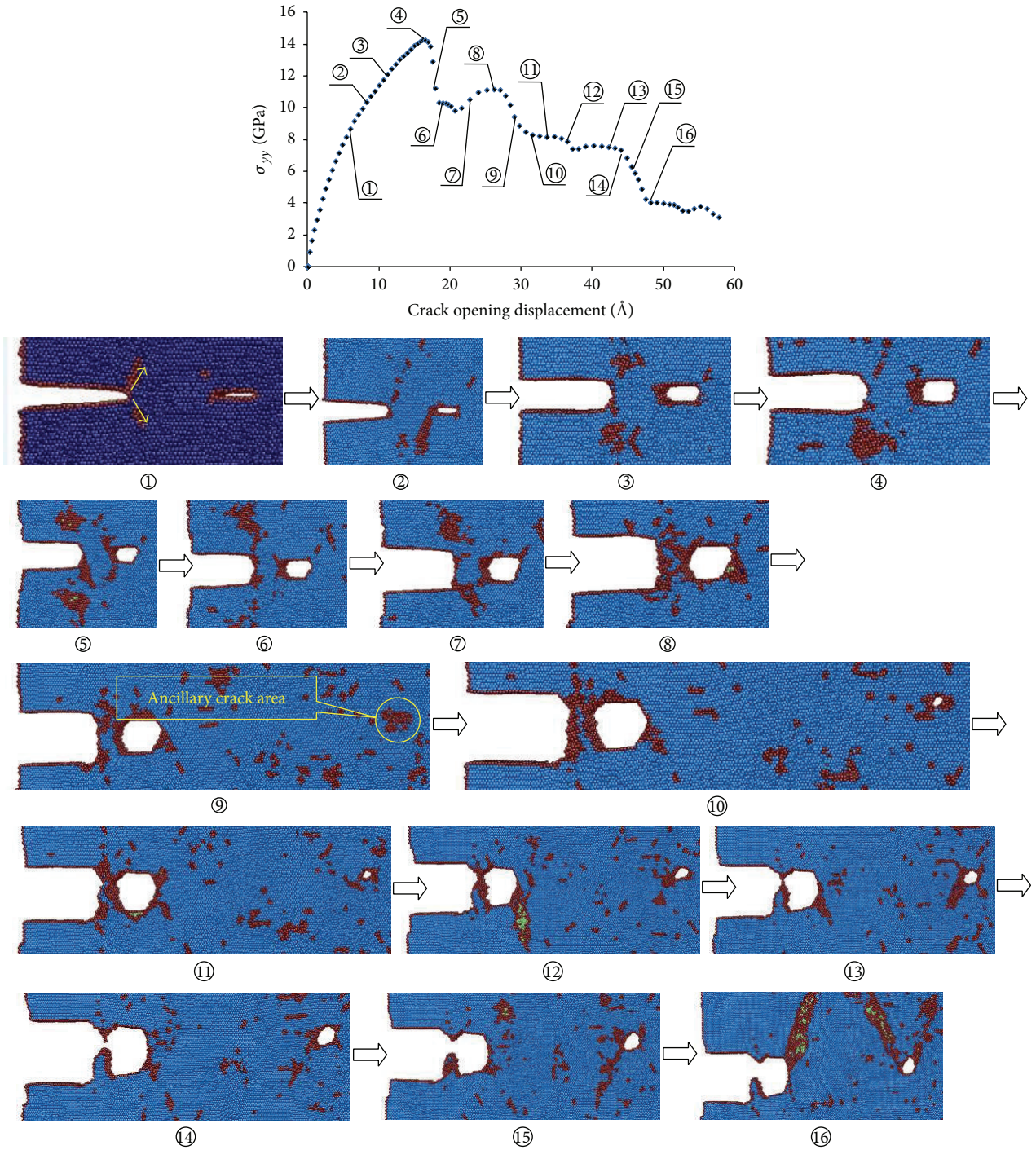

Figure 10: Traction-separation relationship and deformed mechanisms of Model III under tensile loading.

decline rapidly. Then because of stress relaxation, the decline rate of stress should be slowed down until full connection of cracks.

(3) The crack tip deformation process of Model III is shown in Figure 10. The crack tip deformation and failure mechanism are bluntness and dislocation emission (as shown in Figure 10①, arrow pointing to the direction of dislocation emission). In Model III, when T-S curve approaches top value, the crack tip shows serious bluntness and expanded dislocation area, and connection atoms of the main and secondary defects show random status. With further bluntness, the gap between the main and secondary defects narrows down, more connecting atoms show random status, and stress declines. Before full connection of the main and secondary defects, stress should have a temporary small amount of increase. When most of the

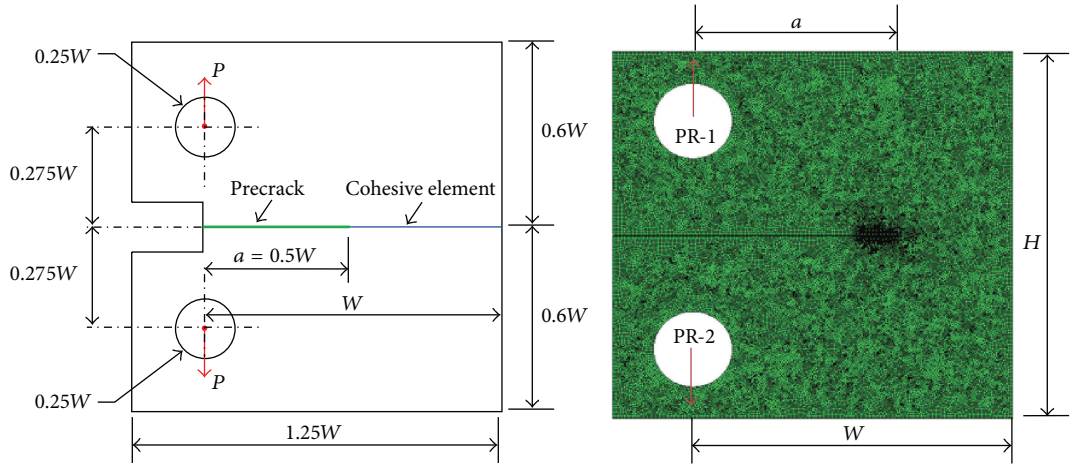

Figure 11: FEM model geometry ($W = 200\,\mu$m) and mesh.

connecting atoms of the main and secondary defects show random status, stress should reach the second top value. With continuous loading, the phase transition area of the ancillary crack (as shown in Figure 10⑨) occurs, and the ancillary crack appears in front of the secondary crack tip with the distance of 5 times the length of the secondary crack. With further loading, the metallic bond of atoms between the ancillary crack phase transition areas is broken, and voids (as shown in Figures 10⑨ and 10⑩), phase transition (BCC, shown in Figure 10⑫), and stress relaxation occur. The rate of stress decline slows down until full connection of the main and secondary defects. With further loading, the front end of new defects forming after full connection of main and secondary defects shows dislocation emission, which makes stress rapidly decline again. When random atoms resulting from dislocation grow obviously, stress relaxation occurs again, and crack propagation rate and stress decline rate both slow down until new defects are formed.

(4) The breakage of the material of α-Ti with microdefects shares certain similarities. The peak value of T-S curve shows that damage starts to occur in the material (crack initialization), and obvious dislocation emission can be shown at the crack tip. After that stress declines rapidly. When plenty of metallic bond of atoms is broken because of stress concentration, most of atoms in the stress concentration area show random status, and then crack shows obvious bluntness, stress relaxes, and the rate of stress decline slows down, which shows flat T-S curve. Before new defect occurs each time, stress should have a temporary small increase, but the top value is smaller than previous top value. After that T-S curve declines rapidly first and then declines slowly. Therefore, multipeak and multiflat can be shown in T-S curve.

(5) T-S curve shows the relationship between surface cohesive force and crack opening displacement. Surface cohesive force increases rapidly along with crack open dislocation first. When peak value is reached, T-S curve declines slowly along with further crack open displacement. For α-Ti material, surface cohesive force shows obvious flat even small rise during declining of T-S curve. The flat of T-S curve is because dislocation leads to more random atoms and makes stress relax. The small rise during declining of T-S curve is because before connection of two cracks, stress is highly concentrated around the cracks, and most energy has to be used to overcome metallic bond energy between atoms around the crack, which makes atoms around the crack show random status. After T-S curve passed peak value (which means damage occurs already), the data dispersion zone in the stress decline period becomes quite wide, which means it is not in a stable status at the initial stage of crack propagation. As further expansion of crack, data dispersion zone becomes more and more narrow, which means crack propagation becomes stable.

(6) T-S curve comprehensively shows the complex deforming mechanisms of crack tip (such as dislocation emission and crack tip bluntness). Hence, it is feasible to take T-S curve, which shows microproperties and is obtained through molecule dynamics as a way to build multiscale computation.

3.3. Simulation of the T-S Fracture Test. In order to model stable crack growth under static loading and analyze cohesive behavior derived from MD towards greater length scales, we performed a simulation of crack growth for a CT specimen subject to displacement loading via prescribed motion of loading pins. Fracture of a CT specimen could verify whether the cohesive law derived from MD simulations displayed behavior consistent with linear elastic fracture mechanics. The geometry and mesh of our CT specimen were shown in Figure 11. The specimen was $1.25W$ wide by $H = 1.2W$ tall, with an effective width (the distance between the pin holes and the uncracked edge) of $W = 200\,\mu$m, an initial crack length of $a = 0.5W$, and pin holes of radius $0.25W$. Cohesive elements were placed along the predefined crack path and were 1 Å wide. The displacement loadings were applied on reference points, that is, PR-1 and PR-2. The parameterized T-S law given was implemented in ABAQUS to simulate the behavior of the cohesive zone model.

After the traction-separation results of the three molecule dynamics models with compound defects got in Part 3.2 were

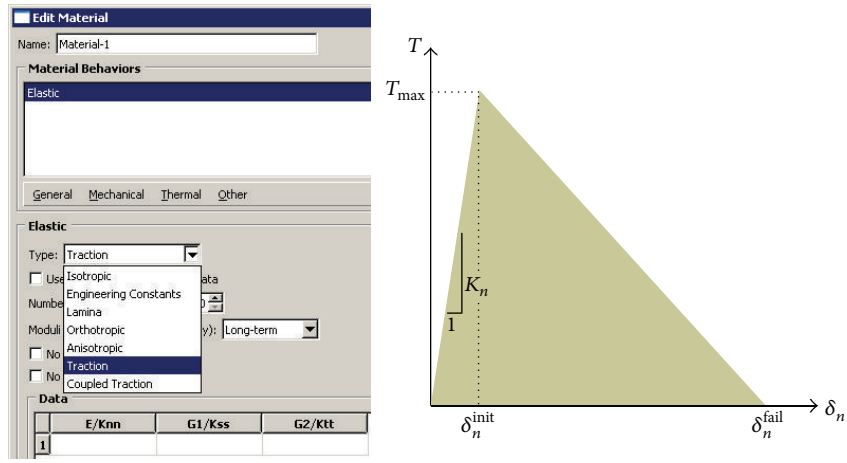

Figure 12: The operation interface of ABAQUAS to simulate the behavior of the cohesive zone model.

made dimensionless, the T-S results could be used in finite element analysis of the specimen showed in Figure 11.

The operation interface of ABAQUAS to simulate the behavior of the cohesive zone model was shown in Figure 12, and three parameters E_n, $T_{\max}$, and δ_n^{fail} should be got from the T-S curve and inputted in ABAQUAS. The rise period and drop period of the T-S curve could be fitted by two lines, and the parameter E_n was the slope of the fitting rising straight line. Then another parameter $T_{\max}$ could be got by

$$T_{\max} = E_n \varepsilon_n = \frac{E_n L \varepsilon_n}{L} = \frac{E_n \delta_n}{L} = K_n \delta_n, \tag{6}$$

where $\delta_n = L\varepsilon_n$, $K_n = E_n/L$ (L is the original thickness of the cohesive element).

The crack opening behavior due to displacement of the top and bottom pins could be observed. Before crack propagation begins to occur, the cohesive zone begins to form. Once a critical displacement was reached, crack propagation was seen in Figure 13. It showed the expected linear relationship between loading-pin displacement and reaction force in Figure 13. More complex fracture mechanics problems could be analyzed through combining the cohesive law derived from MD simulations and finite element method.

Figures 13 and 14 can lead to the following conclusions.

(1) The three microdefects (blunt crack, void, and sharp crack) all have impact on the maximal stress of the macrocrack tip, stress distribution, and stress intensity factor. For the impact extent on stress intensity factor, the largest impact is on blunt crack, followed by void, and the slightest impact is on sharp crack.

(2) Various microdefects properties of materials can be shown in T-S curve, which means that it is feasible to use TSL method to describe the impact of microdefects on the macroproperties of materials.

(3) TSL method can be applied to analyze the impact of microdefects on macro stress intensity factor, fracture ductile, and other fracture factors.

4. Conclusions

(1) Within effective impact area of the crack, a T-S curve consists of rise period and drop period. Curve in rise period is changing linearly, which means the deformation in this period is in elastic period. At this point of time, the crystal lattice size is changing, but nearly no metallic bond breaks. However, in stress drop period, necking phenomenon can be seen because of frequent dislocation and plenty of metallic bonds break.

(2) The maximal stress is related to crack forms and distance between the area and the crack. At the bottom area of the crack, T-S curve shows random status, and the atomic stress is low.

(3) Along the direction of crack propagation and within the effective impact area of the crack, when the distance between the area and the crack tip increases, the gradient of T-S curve in the stress drop period is increasing first but decreasing later, which means the speed of metallic bond break is fast first and slow later. The biggest gradient area in the stress drop period of T-S curve is not in the area of the crack tip, but in the area in front of the crack tip.

(4) The impact area of the crack is approximately 6 times the length of the crack, which means the reasonable T-S area should be within the range of 6 times the length of the crack.

(5) The peak value of T-S curve shows that damage starts to occur in the material (crack initialization), and obvious dislocation emission can be shown at the crack tip. After that stress declines rapidly. When plenty of metallic bond of atoms is broken because of stress concentration, most of atoms in the stress concentration area show random status, and then crack shows obvious bluntness, stress relaxes, and the rate of stress decline slows down, which shows flat T-S curve. Before new defect occurs each time, stress should have a temporary small increase, but the top value is smaller than previous top value. After that T-S curve declines rapidly first and then decline slowly. Therefore, multipeak and multiflat can be shown in T-S curve.

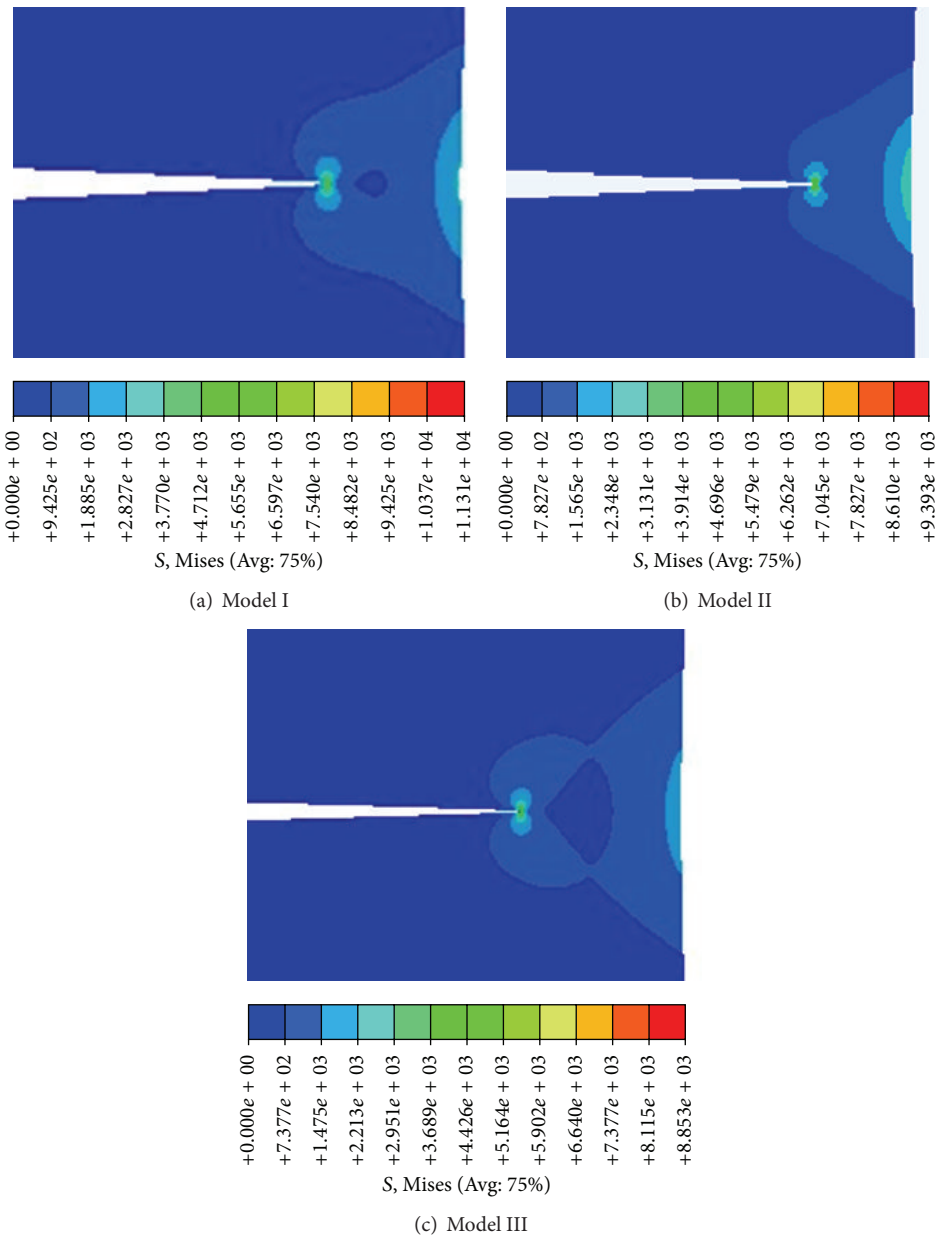

Figure 13: Static crack growth and Mises stress (MPa) contour of the specimen.

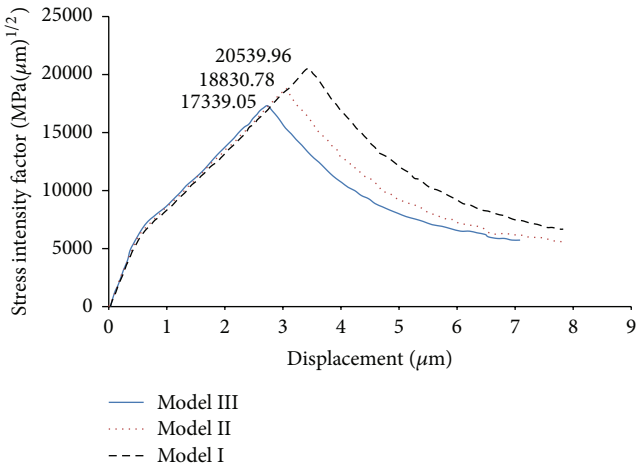

Figure 14: Stress intensity factor of the specimen (three models).

(6) T-S curve shows the relationship between surface cohesive force and crack opening displacement. Surface cohesive force increases rapidly along with crack open dislocation first. When peak value is reached, T-S curve declines slowly along with further crack open displacement. For α-Ti material, surface cohesive force shows obvious flat even small rise during declining of T-S curve. The flat of T-S curve is because dislocation leads to more random atoms and makes stress relax. The small rise during declining of T-S curve is because before connection of two cracks, stress is highly concentrated around the cracks, and most energy has to be used to overcome metallic bond energy between atoms around the crack, which makes atoms around the crack show random status. After T-S curve passed peak value (which means damage occurs already), the data dispersion zone in the stress decline period becomes quite wide, which means it is not in a stable status at the initial stage of crack propagation. As further expansion of crack, data dispersion zone becomes more and more narrow, which means crack propagation becomes stable.

(7) The three microdefects (blunt crack, void, and sharp crack) all have impact on the maximal stress of the macrocrack tip, stress distribution, and stress intensity factor. For the impact extent on stress intensity factor, the largest impact is on blunt crack, followed by void, and the slightest impact is on sharp crack.

Competing Interests

The authors declare that they have no competing interests.

Acknowledgments

This work was supported by the National Defense Basic Scientific Research Program of China through the contract of B1520132013-1 and Key Laboratory of Energy Engineering Safety and Disaster Mechanics, Ministry of Education, entitled the multiscale behavior research of interface performance between metal matrix and nanostructured ceramic coatings.

References

[1] C. Y. Wang and X. Zhang, "Multiscale modeling and related hybrid approaches," *Current Opinion in Solid State and Materials Science*, vol. 10, no. 1, pp. 2–14, 2006.

[2] D. Raabe, *Computational Materials Science: The Simulation of Materials, Microstructures and Properties*, Wiley-VCH, Weinheim, 1998.

[3] J. M. Guedes and N. Kikuchi, "Preprocessing and postprocessing for materials based on the homogenization method with adaptive finite element methods," *Computer Methods in Applied Mechanics and Engineering*, vol. 83, no. 2, pp. 143–198, 1990.

[4] F. F. Abraham, J. Q. Broughton, N. Bernstein, and E. Kaxiras, "Spanning the continuum to quantum length scales in a dynamic simulation of brittle fracture," *Europhysics Letters*, vol. 44, no. 6, pp. 783–787, 1998.

[5] E. B. Tadmor, M. Ortiz, and R. Phillips, "Quasi-continuum analysis of defects in solids," *Philosophical Magazine A*, vol. 73, no. 6, pp. 1529–1563, 1996.

[6] R. E. Rudd and J. Q. Broughton, "Coarse-grained molecular dynamics and the atomic limit of finite elements," *Physical Review B—Condensed Matter and Materials Physics*, vol. 58, no. 10, pp. R5893–R5896, 1998.

[7] N. S. Ottosen, M. Ristinmaa, and J. Mosler, "Fundamental physical principles and cohesive zone models at finite displacements—limitations and possibilities," *International Journal of Solids and Structures*, vol. 53, no. 15, pp. 70–79, 2015.

[8] E. D. Reedy Jr., "Cohesive zone finite element analysis of crack initiation from a butt joint's interface corner," *International Journal of Solids and Structures*, vol. 51, no. 25-26, pp. 4336–4344, 2014.

[9] H. R. E. Houachine, Z. Sereir, B. Kerboua, and K. Hadjazi, "Combined cohesive-bridging zone model for prediction of the debonding between the FRP and concrete beam interface with effect of adherend shear deformations," *Composites Part B: Engineering*, vol. 45, no. 1, pp. 871–880, 2013.

[10] R. Kebriaei, I. N. Vladimirov, and S. Reese, "Joining of the alloys AA1050 and AA5754—experimental characterization and multiscale modeling based on a cohesive zone element technique," *Journal of Materials Processing Technology*, vol. 214, no. 10, pp. 2146–2155, 2014.

[11] D. M. Grogan, C. M. Ó. Brádaigh, and S. B. Leen, "A combined XFEM and cohesive zone model for composite laminate microcracking and permeability," *Composite Structures*, vol. 120, pp. 246–261, 2015.

[12] M. Peters, *Titanium and Titanium Alloys*, Wiley-VCH, Weinheim, Germany, 2003.

[13] S. Plimpton, "Fast parallel algorithms for short-range molecular dynamics," *Journal of Computational Physics*, vol. 117, no. 1, pp. 1–19, 1995.

[14] J. Li, "AtomEye: an efficient atomistic configuration viewer," *Modelling and Simulation in Materials Science and Engineering*, vol. 11, no. 2, pp. 173–177, 2003.

[15] D. S. Dugdale, "Yielding of steel sheets containing slits," *Journal of the Mechanics and Physics of Solids*, vol. 8, no. 2, pp. 100–104, 1960.

[16] G. I. Barenblatt, "The mathematical theory of equilibrium cracks in brittle fracture," *Advances in Applied Mechanics*, vol. 7, pp. 55–129, 1962.

[17] V. Tvergaard, "Effect of fibre debonding in a whisker-reinforced metal," *Materials Science and Engineering A*, vol. 125, no. 2, pp. 203–213, 1990.

[18] P. H. Geubelle and J. S. Baylor, "Impact-induced delamination of composites: a 2D simulation," *Composites Part B: Engineering*, vol. 29, no. 5, pp. 589–602, 1998.

[19] H. Krull and H. Yuan, "Suggestions to the cohesive traction-separation law from atomistic simulations," *Engineering Fracture Mechanics*, vol. 78, no. 3, pp. 525–533, 2011.

[20] X.-P. Xu and A. Needleman, "Numerical simulations of fast crack growth in brittle solids," *Journal of the Mechanics and Physics of Solids*, vol. 42, no. 9, pp. 1397–1434, 1994.

[21] C. Z. Wu, X. W. Li, X. Huang, J. M. Ma, and C. X. Cao, "Relationship of fatigue crack propagation and microstructure for TA15 alloy," *Rare Metal Materials and Engineering*, vol. 36, no. 12, pp. 2128–2131, 2007.